Optically-Regulated Impedance-Based Balancing for Humanoid Robots

Emmanouil Spyrakos-Papastavridis, Dimitrios Kanoulas, Nikos G. Tsagarakis,
and Darwin G. Caldwell

***Abstract*—This paper attempts to resolve the issue of regulating a humanoid robot's impedance levels and Centre-of-Mass (CoM) position, for the purpose of maintaining balance, by means of receiving visual feedback from its environment. Once endowed with visual perception, the robot is rendered capable of ascertaining whether a moving object located within fair proximity to its structure could potentially menace its state of balance, based on its relative distance and velocity. The real-time detection of such an event then necessitates the performance of a preparative action that would serve the purpose of ensuring the system's timely balancing. However, the latter may be viewed as a twofold problem in this context, since in addition to triggering a motion aimed at transferring the CoP towards the side of the polygon at which an external impact is imminent, the robot's impedance also needs to vary appropriately in order to absorb this disturbance. Experimental results obtained using a depth ASUS Xtion PRO Live camera attached to the COmpliant huMANoid (COMAN), clearly demonstrate the balance augmentation that is achievable when incorporating visual feedback into a balancing controller, thus partially corroborating the generic hypothesis that visual perception could potentially pave the way for a bipedal robot's emulation of human-like balancing.**

I. Introduction

LEGGED robotic systems are considered to be amongst the most complicated of artificial machines, due mainly to their numerous Degrees-of-Freedom (DoFs), high Centre-of-Mass (CoM) positions, and diminutive support polygons, thus rendering their balance maintenance an intricate task. It is for this very reason that an immense amount of works in the pertinent literature, attempt to mathematically define the notion of balance via the existence of a single physical quantity. This could manifest itself as either the Zero-Moment-Point (ZMP) [1] or the Centre-of-Pressure (CoP), with both variables representing points that are capable of determining a legged system's overall balance, when relating them to the dimensions of their support polygons. Naturally, the afore-described criteria have been utilized extensively in the development of walking and balancing controllers for legged robots [2].

Nevertheless, the regulation and monitoring of these balance criteria alone, might prove to be insufficient in terms of achieving a desirable level of task execution performance. Therefore, the devise of appropriate control techniques to accompany balance-regulation controllers, could significantly improve the overall stabilization capability of

E. Spyrakos-Papastavridis, D. Kanoulas, N. G. Tsagarakis and D. G. Caldwell are with the Department of Advanced Robotics, Istituto Italiano di Tecnologia, via Morego, 30, 16163 Genova, Italy {emmanouil.spyrakos, dimitrios.kanoulas, nikos.tsagarakis, darwin.caldwell} at iit.it

Figure 1. COMAN preparing for an impact with the ball pendulum.

legged machines. An archetypal example of such a method is undoubtedly impedance control [3], whereby the user is offered the possibility of regulating the system's impedance to appropriate levels, in accordance with the requirements of a specific task. The design and implementation of such control techniques for/to humanoid robots is reported on in [4,5,6], with [4] presenting an impedance controller for a bipedal robot that aims at increasing the swing leg's foot and hip impedance parameters drastically when coming into contact with the environment, in order to absorb the landing forces and maintain stability. An analogous control strategy for humanoid walking is described in [5], wherein the system's compliance is increased immediately before an impact with the ground occurs, followed by a considerable increase of the damping once either of the robot's feet have actually touched down. [6] also focuses on the development of a systematic, analytical approach for the regulation of the system's impedance during the various walking phases.

Low cost range sensors that provide high quality data in real-time, i.e. 30 frames per second (fps), are readily available, making visual 3D perception one of the basic tools for exteroceptive sensing in robotics [7]. It is only natural to then aim at merging vision with balancing, in order to acquire visually-inspired balancing strategies which should, on a theoretical level, outperform their visually deprived counterparts. As far as ZMP-based visual balancing algorithms are concerned, [8] describes a methodology that allows for the integration of 3D vision, motion planning, and bipedal control, whilst simultaneously satisfying ZMP-related constraints. A similar approach that incorporates model predictive control for the purpose of modifying the footsteps, CoM and CoP, is proposed in [9]. It has also been demonstrated however, that non-ZMP-based algorithms could lead to equally as impressive results, as attests the work presented in [10], which entails the use of a high-speed camera to adjust a robot's posture in real-time, thereby allowing it to perform high-speed running.

An additional steppingstone to the achievement of robust and reliable balancing strategies, is the fusion of visual

Preprint submitted to 2015 IEEE-RAS International Conference on Humanoid Robots.
Received July 9, 2015.

perception and impedance control, as was previously stated. One of the earliest works dealing with the resolution of this problem [11], describes the design of an impedance controller whose functionality is contingent upon the amalgamation of visual servo control and force feedback, wherein the visual system is responsible for the provision of reference trajectories, rather than for gain tuning. Such visual impedance control strategies have also been implemented on humanoid robots, in order to ensure safe human-robot interaction and collaboration [12].

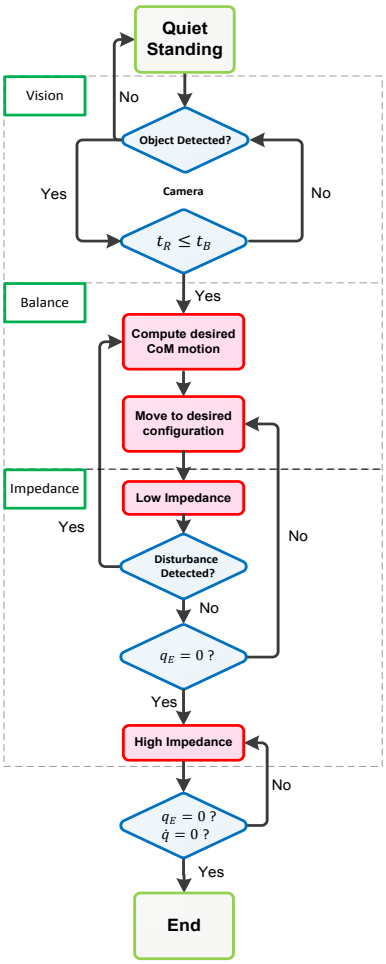

Figure 2. Vision-balance-impedance scheme flowchart.

Finally, the ultimate goal of achieving a triple integration of balancing, visual perception and impedance control, has been realized in [13,14]. In fact, [13] is concerned with a humanoid's performance of an appropriately timed bat swing that ensures the timely strike of an incoming baseball, with its whole body balance being catered for by an impedance control scheme that accounts for the robot's CoP constraints. [14] on the other hand, exploits a visual system, together with an impedance controller that permits the regulation of the active stiffness and damping parameters of a biped's legs, thus enabling the robot's successful engagement in a game of table tennis.

The work to be presented in this paper, describes the merging of visual perception, balancing and impedance tuning, into a single framework (Fig. 2) aimed at augmenting a humanoid system's balancing capability. Consequently, a set of experiments entailing a robot's perturbation by means of a ball pendulum released at varying heights from the ground (Fig. 1), demonstrate that the visually endowed algorithm proposed herein, significantly outperforms the visually deprived method that it has been compared to.

The rest of the paper is structured as follows; section II describes the dynamics of an over-actuated compliant system, section III presents the visual perception system, section IV is concerned with the balance and timing issues, section V reports on the impedance regulation method, and finally section VI discusses the conclusions.

II. Dynamics and Stability Of Over-Actuated Compliant System

For a compliant humanoid standing in double support, a generic j-degree of freedom robot is considered, possessing n_i-drives for each degree of freedom $i = 1,2 \dots j$. The total number of drives is $n = \sum_{i=1}^{j} n_i$, and thus the link and motor dynamics may be described as follows [15]:

$$M_J(q)\ddot{q} + C(q,\dot{q})\dot{q} + S_m^T K(S_m q - \theta) = \tau_g(q) + \tau_{ex}, \quad (1)$$

$$J\ddot{\theta} + D\dot{\theta} + K(\theta - S_m q) = \tau_m, \quad (2)$$

where q and θ are the link and motor positions, $M_J(q)$ and $C(q,\dot{q}) \in \mathbb{R}^{j \times j}$ are the inertia and Coriolis/centripetal matrices respectively, $\tau_g(q)$ is the gravity torque vector, τ_m is the actuation torque vector and τ_{ex} is the vector of external forces. $K \in \mathbb{R}^{n \times n}$ is a diagonal matrix with positive entries representing the passive spring stiffness between the motors and the robot links, while $J, D \in \mathbb{R}^{n \times n}$ are the motor inertia and damping. S_m is a selection matrix that serves the purpose of selecting the appropriate actuators for every link.

However, the over-actuated nature of the double support stance leads to the six joints being treated as three, although all six actuators are considered. The elements of the 3-DOF double support vector are arranged as follows:

$$\tau_g = [\tau_{ga} \quad \tau_{gk} \quad \tau_{gh}]^T \quad (3)$$

with $\tau_{ga}, \tau_{gk}, \tau_{gh}$ representing the ankle, knee and hip torques respectively. One of the main properties of the gravity vector, to be used in subsequent sections is:

$$\left\| \frac{\partial \tau_g(q)}{\partial q} \right\| = \left\| \frac{\partial^2 U_g(q)}{\partial q^2} \right\| \leq \alpha \quad (4)$$

for some $\alpha > 0$; wherein $U_g(q)$ denotes the potential energy due to gravity, $\tau_g(q) = -\left(\partial U_g(q)/\partial q\right)^T$ and the operator norm $\|A\| = max\{\|Ax\|/\|x\|\}$ is considered.

The low-level joint controller was based upon gravity compensation control, employing motor feedback. The associated control law may be represented as follows [15]:

$$\tau_m = K_P(S_m q_d - \theta) - K_D\dot{\theta} + u_{gc}, \quad (5)$$

where q_d is the desired position, K_P, K_D are the diagonal, positive definite motor position and motor velocity feedback gain matrices, while u_{gc} contains gravity-related terms. By considering the closed-loop system's steady state equations, we can define the following matrix that plays a central role in the stability analysis since its satisfaction of certain conditions ensures uniqueness of the equilibria [16]:

$$T_D = \begin{bmatrix} S_m^T K S_m & -S_m^T K \\ -K S_m & K_P + K \end{bmatrix}. \quad (6)$$

Thus the condition expressed by (4) can be described as follows:

$$\lambda_m(T_D) \geq \alpha, \quad (7)$$

where $\lambda_m(.)$ denotes the minimum eigenvalue/value of a given matrix/vector. The following Lyapunov function shall be considered throughout the paper:

$$V_T(q_F, \dot{q}_F) = \frac{1}{2}\dot{q}_F^T M(q)\dot{q}_F + \frac{1}{2}q_E^T T_D(t) q_E + U_g(q) - U_g(q_d) + q_E^T \begin{bmatrix} \tau_g(q_d) \\ 0 \end{bmatrix} \geq 0, \quad (8)$$

with $q_F = \begin{bmatrix} q \\ \theta \end{bmatrix}$, $q_{F_d} = \begin{bmatrix} q_d \\ \theta_d \end{bmatrix}$, $q_E = (q_F - q_{F_d})$, $M = \begin{bmatrix} M_J(q) & 0 \\ 0 & J \end{bmatrix}$. The above function's time derivative is the following:

$$\dot{V}_T(q, \theta) = -\dot{q}_F^T \cdot \eta \cdot \dot{q}_F + \frac{1}{2}q_E^T \dot{T}_D(t) q_E, \quad (9)$$

ensuing a series of calculations that have been omitted, where $\eta = \begin{bmatrix} 0 & 0 \\ 0 & D + K_{m2} \end{bmatrix}$. In this case, stability is guaranteed if and only if:

$$\dot{q}_F^T \cdot \eta \cdot \dot{q}_F \geq \frac{1}{2}q_E^T \dot{T}_D(t) q_E, \quad (10)$$

which implies that the system can potentially be destabilized by increases in the robot's overall stiffness value denoted by $T_D(t)$, although this is not an issue when considering decreasing values of this matrix, since in that case the potential energy term adopts a negative sign.

III. Balance Maximization Technique

A. Visual 3D Perception

Object detection and tracking have been studied extensively over the last few years, using both 2D and 3D visual data (see for example the survey in [17]). In this work, we assume a moving object in a static environment and we detect and track it using a combination of an optical-flow based background removal [18] on the RGB image and a color-based segmentation algorithm to reduce the noise that may appear due to little variations in color, such as the object's shadow. In particular, an ASUS Xtion PRO Live range sensor has been attached to the robot in such a way that the image plane goes through the center of mass of the robot and provides 640x480 RGB-D data in 25 fps.

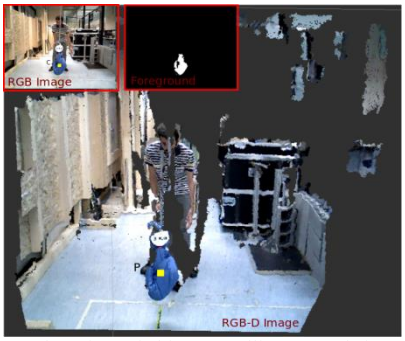

Figure 3. Robot view of object travelling towards its structure.

For each frame we apply the Gaussian mixture-based background filtering algorithm introduced in [18] on the RGB image, using 3 Gaussian mixtures followed by a simple erosion, dilation, and blurring for the purpose of reducing the noise. After this process we end up with the pixels that correspond to the moving object (foreground, Fig. 3, upper right) in the environment. Due to the object's shadow and other small variations in the RGB image between two consecutive frames, we also apply a color-based filtering to remove them. We get the 2D centroid pixel C of the moving object in each RGB frame:

$$C = \left\{\frac{M_{10}}{M_{00}}, \frac{M_{01}}{M_{00}}\right\} \in \mathbb{R}^2 \quad (11)$$

where M_{10}, M_{01}, M_{00} are the second order moments of the foreground pixels in the RGB image (Fig. 3, upper left). We then calculate the 3D position $P \in \mathbb{R}^3$ of the object (Fig. 3) using a small neighborhood of the corresponding C pixel in the depth image for each frame. The object recognition and tracking is implemented in C++ using the Open Source Computer Vision (OpenCV) and the Point Cloud (PCL) [7] Libraries, and takes roughly 35ms per frame. Having the position of the object in each frame we can easily compute the velocity, v, and acceleration, α, over a sequence of five consecutive frames.

B. Elastic-Collision-based CoM regulation

The majority of balance criteria, such as the CoP and ZMP, describe points that are defined within a system's convex hull of contacts. It is then reasonable to assume that in the absence of visual feedback, which renders the robot agnostic to a prospective disturbance's direction of motion, the system's balance can be 'maximized' by aiming to transfer its CoP to a point that is equidistant from both of the support polygon's edges. Contrarily, when the robot is capable of ascertaining an impending perturbation's direction of motion, it could potentially elect to regulate its CoP based on visual feedback, thus capitalizing on additional data pertaining to the object's motion, in this case, its velocity and acceleration. If an elastic impact is assumed to occur

between the object and the robot (Fig. 4 left), it could then be concluded that the object's kinetic energy is converted into elastic potential energy, such that:

$$\frac{1}{2}m_o v^2 = \frac{1}{2}K_s x^2, \tag{12}$$

with m_o and v being the object's mass and velocity respectively, while K_s and x denote the elastic component's stiffness and displacement. The duration of the robot-object impact could then be computed by means of solving the following quadratic equation:

$$x = vt + \frac{1}{2}\alpha t^2 \tag{13}$$

analytically with respect to time, t, whilst assuming that x has already been computed using the previous equation. The initial robot CoM velocity that will ensue the impact, could be divided using the previously calculated t variable, thereby yielding the resulting CoM acceleration, $\ddot{x}_{CoM}$, which could in turn be inserted into the following LIPM-related formula:

$$x_{CoM} = x_{CoP} + \frac{z_{CoM} \cdot \ddot{x}_{CoM}}{g}, \tag{14}$$

, where g is the gravitational acceleration constant, x_{CoM} and z_{CoM} denote the x and z-axis CoM positions respectively, z_{CoM} is a fixed CoM height, while x_{CoP} is the x-axis CoP position. Given that the x_{CoP} value could be directly acquired by virtue of the FT sensors at the robot's feet, then the above equation shall provide the required CoM motion, which could be straightforwardly translated into joint references.

C. Trigger Time Computation

In order to congrue with the theory, equation (14) should provide a single set of references, since the closed-loop system is theoretically capable of performing mere regulation tasks. Therefore, an additional twofold problem is to be addressed within this subsection, since the controller should firstly provide a reference position expressed through equation (14), in order to transfer the robot's CoM to an appropriate location, while it should then provide a reference corresponding to a favorable CoP position of maximal balance. In order to successfully tackle the former problem, the derivation of an accurate position reference alone is not necessarily conducive to the robot's attainment of a balanced state, since this desired configuration might never materialize if the velocity magnitude of the impending object is such that an impact with the robot will transpire before the robot's CoP manages to reach the edge of the polygon. Therefore, the timing of this reference activation is crucial in the overall operation of the scheme, as it directly determines whether or not the target position is to be reached. To this end, a relationship between the closed-loop system's response time and the object's distance and velocity from the robot, ought to be established. It may be assumed that the time (t_{res}) taken for the humanoid to move its joints from rest (starting at time $t = t_{init}$) to a predefined position, which shall be represented by x_P, could be computed beforehand either via simulations or experimentally. In addition to this array of robot-specific information, the visual perception algorithm would then provide similar data regarding the ball's motion, namely its distance from the x_P position, denoted by x_B, and its instantaneous velocity, v, which could be expressed as follows:

$$t_B = \frac{|x_P - x_B|}{v} \tag{15}$$

hence yielding an equation describing the time taken for the ball to strike the robot. As long as the sum of the initial time and the closed-loop system's response time, does not exceed t_B, as shown below:

$$t_{init} + t_{res} \leq t_B, \tag{16}$$

then the robot is guaranteed to reach the desired state intact (Fig. 4 right).

In order to compute a triggering time based on this inequality, a safety margin, γ_M, is introduced to the equation as shown below:

$$t_R = t_T, \tag{17}$$

where $t_T = \frac{t_B}{\gamma_M}$ with $0 < \gamma_M < 1$, and $t_R = t_{init} + t_{res}$. Note that the safety margin's magnitude defines the conservativeness of the triggering condition.

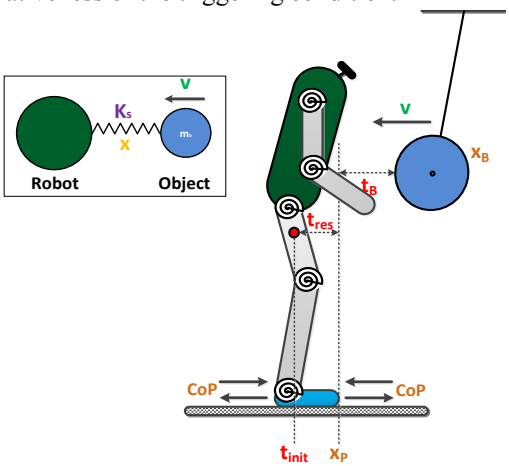

Figure 4. Elastic collision (left) and trigger time (right).

Once the robot has been perturbed, its CoM will inevitably be displaced to a position away from the polygon edge, although the extent to which it will do so shall vary in accordance with both the impact's magnitude, and the system's impedance. Nevertheless, the robot should ideally switch its reference position once a disturbance has been detected, in order to ensure that it will come to rest at a position determined by equation (14). The robot would be capable of ascertaining whether it has been perturbed by an external impact via the real-time measurement of its

Preprint submitted to 2015 IEEE-RAS International Conference on Humanoid Robots.
Received July 9, 2015.

Lyapunov energy, since this quantity would indicate either a convergence or divergence from the desired equilibrium point. The energy variation between samples, E_{SGN}, can be monitored online as this would provide the pertinent information, i.e. the robot diverges when $E_{SGN} > 0$ and it converges when $E_{SGN} < 0$. Thus, the value of the relationship provided below:

$$E_{SGN} = sgn\big(V_T(i) - V_T(i-1)\big), \tag{18}$$

is monitored online to determine the robot's state of balance. Evidently, the rate at which the convergence to such a position occurs, depends on the magnitude of the disturbance force, the actuated and unactuated dynamics, and the controller action.

IV. Optically-triggered Impedance Regulation

A. Active Stiffness Tuning: Convergent Case

One should ideally attempt to regulate the system's stiffness in a manner that leads both to a satisfaction of the stability criteria described by (9), as well as to an achievement of the desired balancing behavior. To that end, a means of ensuring rapid convergence to the desired equilibrium would be through an increase of the system's overall stiffness, although the energy injection that would ensue could exacerbate the robot's state of balance, as was previously described. However, this energy injection phenomenon could potentially be eliminated by electing to increase the system's overall stiffness only once the position error is equal to zero, since in that case:

$$q_E^T \dot{T}_D(t) q_E = 0 \text{ for } q_E = 0 \tag{19}$$

Despite the theoretical absence of a restriction on the magnitude of the active stiffness, it is in a practical sense essential to contrive an upper bound for the value of this parameter, given the physical power-related limitations. For this purpose, an upper bound can be acquired by computing the K_P gain magnitude that would cause controller saturation, assuming that the saturation damping gain can be represented in the following manner:

$$k_{D_{max}} = 2\xi_d \sqrt{\|J\| \left\| k_{P_{max}} \right\|}, \tag{20}$$

with ξ_d being the desired damping ratio, while $k_{P_{max}}$ is the maximum active stiffness value. Inserting (20) into (5), while taking the norms of the terms on both sides of the equation and considering only the equality condition, yields:

$$\begin{aligned} \| \tau_m\| = \left\| k_{P_{max}} \right\| \|q_E\| + \left\| u_{gc} \right\| \\ +2\xi_d \sqrt{\|J\| \left\| k_{P_{max}} \right\|} \left\| \dot{\theta} \right\|, \end{aligned} \tag{21}$$

where the value of $\| \tau_m\|$ is known beforehand, as it denotes the maximum actuation torques that could be provided without causing saturation, whereas $\left\| \dot{\theta} \right\|$, $\|q_E\| = \|S_m q_d - \theta\|$ and $\left\| u_{gc} \right\|$ are computed using the sensory measurements. Substituting $A^2 = \left\| k_{m1_{max}} \right\|$ leads to the following:

$$A^2 \|q_E\| + A\left(2\xi_d \sqrt{\|J\|} \left\| \dot{\theta} \right\|\right) + \left(\left\| u_{gc} \right\| - \| \tau_m\|\right) = 0$$

Since the above equation is quadratic, it can be solved immediately, although the discriminant's positiveness needs to be verified, on the basis of the standard quadratic equation solution, in order to ensure the generation of real solutions:

$$\xi_d^2 \left\| \dot{\theta} \right\|^2 \|J\| - \|q_E\| \left\| u_{gc} \right\| + \|q_E\| \| \tau_m\| > 0 \tag{22}$$

Given that $\| \tau_m\| > \left\| u_{gc} \right\|$, then the formula shall produce real solutions and thus (22) can be used to generate $\left\| k_{P_{max}} \right\|$ values, setting $\xi_d = 1$ for the convergent case.
Since however, the product of this set of operations shall be a scalar value, a dynamics-based distribution of the gains across the joint space is necessary. Hence, the following array of gravitational vector weights is defined, as it is capable of performing a sound distribution of the gains:

$$W_K = diag\left(\frac{w_k}{\|w_k\|}\right), \text{ where } w_k = S_m \begin{bmatrix} \frac{\tau_{ga}}{\tau_{gT}} & \frac{\tau_{gk}}{\tau_{gT}} & \frac{\tau_{gh}}{\tau_{gT}} \end{bmatrix} \tag{23}$$

B. Active Stiffness Tuning: Divergent Case

In contrast to the stability issues caused by increasing the active stiffness values, the lowering of these values has absolutely no detrimental effect on the system's stability, as clearly expressed via equation (10). Therefore, the proportional gain could be instantaneously decreased to an arbitrarily low value, so long as equation (7) is satisfied. Based on this restriction, in addition to the fact that (7) may be expressed as follows[1]:

$$\lambda_m(H(K_P)) \geq \alpha - \lambda_m(K_T), \tag{24}$$

then the minimum allowable stiffness value may be computed through the relationship:

$$k_{P_{min}} = \big(\alpha - \lambda_m(K_T)\big). \tag{25}$$

wherein,

$$K_T = \begin{bmatrix} S_m^T K S_m & -S_m^T K \\ -K S_m & K \end{bmatrix}, \tag{26}$$

while the matrix function $H(.)$ constructing a 9×9 matrix from the 6×6 matrix (.), is expressed via the equation:

$$H(K_P) = \begin{bmatrix} 0 & 0 \\ 0 & K_P \end{bmatrix}. \tag{27}$$

Once again, the gains could be distributed across the joints using equation (23).

[1] It can be shown that $\lambda_m(\rho + \chi) \leq \lambda_m(\rho) + \lambda_m(\chi)$ ([19]).

Preprint submitted to 2015 IEEE-RAS International Conference on Humanoid Robots.
Received July 9, 2015.

C. Active Damping Tuning: Convergent/Divergent Cases

Regardless of the fact that the derivative gains are unable to affect the system's stability (on a theoretical level), the fashion in which they are to be distributed to the various joints, requires prudent planning. For the convergent case, the damping saturation value is straightforwardly calculated using equation (20), although this is contingent upon the existence of a stiffness saturation value, $k_{P_{max}}$. Nevertheless, once a $k_{D_{max}}$ value has been successfully obtained, it may then be multiplied by the following weighting vector:

$$W_D = \frac{\sqrt{J \cdot K_P}}{\sqrt{\|J \cdot K_P\|}} \tag{28}$$

which shall once again guarantee an intuitive gain distribution. In an analogous fashion, the gains for the divergent case may be computed using a modified version of (20), possessing the following form:

$$k_{D_{min}} = 2\xi_d \sqrt{\lambda_{min}\left(J \cdot k_{P_{min}}\right)}, \tag{29}$$

yielding a result that necessitates a multiplication by the weighting matrix described by (28).

V. Optical Balancing Tests

A. Experimental Setup

The COMAN (Fig. 1) comprises 25 DoF's with a weight and height of 31.2 kg and 0.945 metres respectively, while 12 of its joints are powered by series elastic actuators. The real-time communication is performed via UDP, using the Ethernet port of an AMD FX™-8350 Eight-Core Processor @ 4 GHz machine.

Figure 5. Robot leaning forward and lowering its impedance.

A series of experiments was carried out (Fig. 5) in order to corroborate the functionality of the impedance regulation techniques described throughout the paper, in addition to the efficacy of the proposed overall balancing scheme. Figs. 6 and 7 display the effect of perturbing the robot when using controllers with fixed high and low impedance gains respectively, while also maintaining a fixed pose about the zero position. The perturbations were applied by means of a ball pendulum attached to the lab's ceiling, which was released from a height that would ensure that the impact would occur at the robot's CoM (at approximately 68 cm), resulting in a CoP motion towards the edge of the support polygon (computed using equations (12)-(14)), thus causing an overturning of the mechanism. Figs. 6 and 7 elucidate the fixed-gain controllers' incapability of absorbing even low magnitude impacts, since their respective CoP's begin from a zero position and then move rapidly towards the edge of the polygon, leading to a fall.

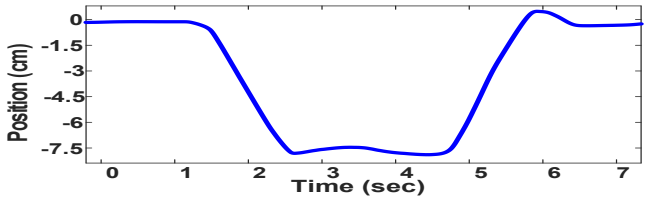

Figure 6. Fixed-gain high impedance controller (constant references)

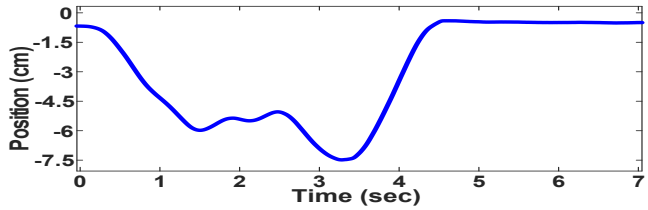

Figure 7. Fixed-gain low impedance controller (constant references)

Subsequently, it was essential to exhibit the balance maximization method's capability of transferring the robot's CoP to a point that lay in close proximity to the support polygon's edges, whilst also regulating the gains appropriately. A fair set of tests involved releasing the ball pendulum from varying heights, performed in 4 cm increments, thereby enhancing the intensity of the impact occurring at the CoM, while the balancing scheme was activated in order to permit the CoP/CoM to move towards an appropriate position (computed using equations (12)-(14)) that would ensure balance maintenance. The various impacts shall be referred to as Low, Low/Moderate, Moderate, High/Moderate and High, with ball heights of 73, 77, 81, 85, 89 cm's respectively. It is noteworthy that the experiments were run successfully ten consecutive times, thus indicating a satisfactory level of repeatability. Fig. 8 depicts the CoP evolutions pertaining to the experiments described in the previous lines, arranged in ascending order of impact magnitudes, while the associated pictures on the RHS of each plot correspond to the final, pre-impact positions attained during the relevant experiments.

Preprint submitted to 2015 IEEE-RAS International Conference on Humanoid Robots.
Received July 9, 2015.

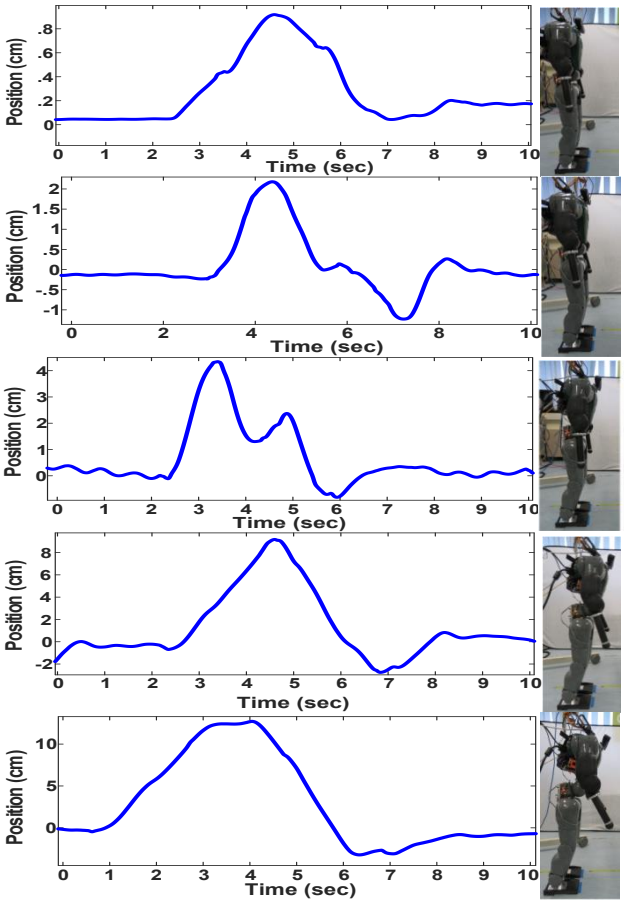

Figure 8. CoP evolution using proposed scheme during experiments (left), and corresponding pre-impact robot positions (right).

The video attachment pertaining to these experiments offers an intelligible demonstration of the afore-mentioned results that are depicted in the above figures, while it may also be viewed in high quality by following the provided link [20].

VI. Conclusions

An impedance regulation scheme, combined with balancing control and visual perception, was presented in this paper for the purpose of enhancing a humanoid robot's balancing capability. The visual data allowed the robot to ascertain the impending object's velocity and distance from its structure, which then served as a trigger for the system's CoM movement towards the edge of the polygon. Moreover, the robot's impedance was lowered upon assuming this maximum stability position, thereby allowing for the absorption of higher external perturbations in a timely fashion. Subsequently, the controller aimed at increasing the system's impedance so as to ensure that the system would come to a halt, or attempt to stabilize itself, at a desired configuration. The results demonstrated via a comparative study, that balancing schemes incorporating visual perception tend to outperform ones that are visually deprived, thus providing a fractional validation of the widely believed postulate that vision could aid the endowment of robotic systems with more human-like behaviour.

VII. Acknowledgement

This work is supported by the WALK-MAN FP7-ICT-2013-10 European Commission project.

References

[1] M. Vukobratovic, B. Borovac, "Zero-moment point – Thirty Five Years of its Life," *Int. J. of Humanoid Robotics, vol. 1, no. 1, pp. 157-173, 2004.*

[2] S. Kajita, M. Morisawa, K. Miura, S. Nakaoka, K. Harada, K. Kaneko, F. Kanehiro and K. Yokoi, "Biped walking stabilization based on linear inverted pendulum tracking," *Proc. IEEE/RSJ Int. Conf. on Intelligent Robots and Systems, pp. 4489-4496, 2006.*

[3] N. Hogan, "Impedance Control: An Approach to Manipulation," *American Control Conference, pp. 304-313, 1984.*

[4] J. H. Park, "Impedance control for biped robot locomotion," *IEEE Trans. on Robotics and Automation, vol. 17, no. 6, pp. 870-882, 2001.*

[5] H.-O. Lim, S. A. Setiawan, A. Takanishi, "Balance and impedance control for biped humanoid robot locomotion," *Proc. IEEE/RSJ Int. Conf. on Intelligent Robots and Systems, pp. 494-499, 2001.*

[6] T. Sugihara, Y. Nakamura, "Contact phase invariant control for humanoid robot based on variable impedant inverted pendulum model," *Proc. IEEE Int. Conf. on Robotics and Automation, vol. 1, pp. 51-56, 2003.*

[7] R. B. Rusu, S. Cousins, "3D is here: Point Cloud Library (PCL)". *Proc. IEEE Int. Conf. on Robotics and Automation, 2011.*

[8] S. Kagami, K. Nishiwaki, J. J. Kuffner Jr, Y. Kuniyoshi, M. Inaba, H. Inoue, "Online 3D vision, motion planning and bipedal locomotion control coupling system of humanoid robot: H7," *Proc. IEEE/RSJ Int. Conf. on Intelligent Robots and Systems, pp. 2557-2562, 2002.*

[9] M. Garcia, O. Stasse, J. B. Hayet, C. Dune, C. Esteves, J. P. Laumond, "Vision-guided motion primitives for humanoid reactive walking: Decoupled versus coupled approaches," *Int. J. on Robotics Research, vol. 34, pp. 402-419, 2015.*

[10] T. Tamada, W. Ikarashi, D. Yoneyama, K. Tanaka, Y. Yamakawa, T. Senoo, M. Ishikawa, "High-speed bipedal robot running using high-speed visual feedback," *Proc. IEEE Int. Conf. on Humanoid Robots, pp. 140-145, 2014.*

[11] G. Morel, E. Malis, S. Boudet, "Impedance based combination of visual and force control," *Proc. IEEE Int. Conf. on Robotics and Automation, pp. 1743-1748, 1998.*

[12] D. Agravante, A. Cherubini, A. Kheddar, "Using vision and haptic sensing for human-humanoid joint actions," *Proc. IEEE Int. Conf. on Robotics, Automation and Mechatronics, pp. 13-18, 2013.*

[13] S. Hyon, J. Moren, G. Cheng, "Humanoid Batting with Bipedal Balancing," *Proc. IEEE Int. Conf. on Humanoid Robots, pp. 493-499, 2008.*

[14] Y. Sun, R. Xiong, Q. Zhu, J. Wu, J. Chu, "Balance Motion Generation for a Humanoid Robot Playing Table Tennis," *Proc. IEEE Int. Conf. on Humanoid Robots, pp. 19-25, 2011.*

[15] E. Spyrakos-Papastavridis, G. Medrano-Cerda, N. G. Tsagarakis, J. S. Dai and D. G. Caldwell, "Gravity Compensation Control of Compliant Joint Systems with Multiple Drives," *Proc. IEEE Int. Conf. on Robotics and Automation, pp.4960-4966, 2013.*

[16] P. Tomei, "A Simple PD Controller for Robots with Elastic Joints," *IEEE Transactions on Automatic Control, vol. 36, pp. 1208-1213 1991.*

[17] A. Yilmaz, O. Javed. M. Shah, "Object Tracking: A Survey", *in ACM Computing Surveys (CSUR), 2006.*

[18] Z. Zivkovic, "Improved Adaptive Gausian Mixture Model for Background Subtraction", *Proc. Int. Conf. Pattern Recognition, 2004.*

[19] T. Tao, "Topics in Random Matrix Theory," *Graduate Studies in Mathematics, Vol. 132, pp. 46-47, 2012.*

[20] http://youtu.be/yFeeIntqxrk